The Astrophysical Journal, 836:77 (17pp), 2017 February 10 https://doi.org/10.3847/1538-4357/836/1/77

Precision Stellar Characterization of FGKM Stars using an Empirical Spectral Library

Samuel W. Yee[1], Erik A. Petigura[1,3], and Kaspar von Braun[2]
[1] California Institute of Technology, USA; syee@caltech.edu
[2] Lowell Observatory, 1400 W. Mars Hill Road, Flagstaff, AZ 86001, USA
Received 2016 November 23; revised 2016 December 30; accepted 2016 December 30; published 2017 February 9

Abstract

Classification of stars, by comparing their optical spectra to a few dozen spectral standards, has been a workhorse of observational astronomy for more than a century. Here, we extend this technique by compiling a library of optical spectra of 404 touchstone stars observed with Keck/HIRES by the California Planet Search. The spectra have high resolution ($R \approx 60{,}000$), high signal-to-noise ratio ($S/N \approx 150$/pixel), and are registered onto a common wavelength scale. The library stars have properties derived from interferometry, asteroseismology, LTE spectral synthesis, and spectrophotometry. To address a lack of well-characterized late-K dwarfs in the literature, we measure stellar radii and temperatures for 23 nearby K dwarfs, using modeling of the spectral energy distribution and *Gaia* parallaxes. This library represents a uniform data set spanning the spectral types ∼M5–F1 ($T_{\rm eff} \approx 3000$–7000 K, $R_\star \approx 0.1$–$16\,R_\odot$). We also present "Empirical SpecMatch" (`SpecMatch-Emp`), a tool for parameterizing unknown spectra by comparing them against our spectral library. For FGKM stars, `SpecMatch-Emp` achieves accuracies of 100 K in effective temperature ($T_{\rm eff}$), 15% in stellar radius ($R_\star$), and 0.09 dex in metallicity ([Fe/H]). Because the code relies on empirical spectra it performs particularly well for stars ∼K4 and later, which are challenging to model with existing spectral synthesizers, reaching accuracies of 70 K in $T_{\rm eff}$, 10% in $R_\star$, and 0.12 dex in [Fe/H]. We also validate the performance of `SpecMatch-Emp`, finding it to be robust at lower spectral resolution and S/N, enabling the characterization of faint late-type stars. Both the library and stellar characterization code are publicly available.

Key words: techniques: spectroscopic

Supporting material: machine-readable tables

1. Introduction

Measuring the physical properties of stars is a long-standing and important problem in astronomy. The masses, radii, and temperatures of stars are benchmarks against which we test models of stellar structure and evolution. The abundances of iron and other elements in stellar populations help trace the nucleosynthetic enrichment history of the Milky Way. Recently, the study of extrasolar planets has placed new demands on *precision* stellar characterization. The extent to which observational methods like radial velocities and transit photometry can reveal a planet's mass and radius is limited by the uncertainty in the host star's mass and radius, respectively.

Eclipsing binaries typically offer the most precise and least model-dependent measurements of stellar mass ($M_\star$) and radius ($R_\star$), relying primarily on Newtonian mechanics and geometry. Analysis of the light curves and radial velocities of eclipsing binaries can achieve measurements of $M_\star$ and $R_\star$ accurate to $\lesssim$3%. After incorporating broadband photometry and parallaxes, eclipsing binaries can yield effective temperatures ($T_{\rm eff}$) accurate to ∼2% (Torres et al. 2010).

Measurements of such stellar properties for isolated field stars are more challenging and rely more heavily on models of stellar interiors and atmospheres. For example, precision space-based photometry from the *Kepler* and *CoRoT* missions (Auvergne et al. 2009; Borucki et al. 2010) has enabled the detection of stellar acoustic modes, which achieve $M_\star$ and $R_\star$ accurate to a few per cent (e.g., Bruntt et al. 2012; Huber et al. 2013). The amplitude of these modes grows with the size of the star and they have been detected in stars that are roughly solar-size or larger. For smaller stars, the acoustic oscillation amplitudes are smaller, making their detection increasingly difficult against photometric noise due to photon Poisson statistics, surface granulation, and other sources of stellar activity. While asteroseismology has provided some excellent stellar benchmarks, it is not applicable for all stellar types. This illustrates a recurring challenge in the field of precision stellar astrophysics: no single technique is uniformly effective across the Hertzsprung–Russell (H–R) diagram.

Recently, optical and infrared interferometry have been used to directly measure the angular size of stars (e.g., von Braun et al. 2014). When combined with parallax measurements and an observed spectral energy distribution (SED), this technique provides $T_{\rm eff}$ and $R_\star$ that are almost purely empirical. Interferometry requires stars that are nearby and bright and is thus currently applicable to only a limited number. As of 2016, only about ∼100 main-sequence stars and ∼200 giants have precision interferometric measurements. Stars cooler than ∼5000 K are underrepresented in this interferometric sample because of their faintness. Finally, obtaining $M_\star$ relies on a spectroscopic measurement of $\log g$ coupled with the directly determined $R_\star$ or on the use of stellar structure models with $T_{\rm eff}$, $R_\star$, and spectroscopic measurements of the star's metallicity as input.

Another common technique for stellar characterization relies on detailed modeling of a star's spectrum. This involves constructing a model stellar atmosphere and modeling the radiative transfer of photons as they emerge from the photosphere on their way toward Earth. The effective temperature, surface gravity ($\log g$), metallicity ([Fe/H]), abundance of other species, and projected rotational velocity ($v \sin i$) are adjusted until the simulated distribution of photons matches the

[3] Hubble Fellow.

observed spectrum. Two commonly used spectral synthesis codes are MOOG (Sneden 1973) and SME (Valenti & Piskunov 1996; Valenti & Fischer 2005; Brewer et al. 2015). One challenge facing spectral synthesis is that model stellar atmospheres grow more uncertain as they diverge from solar. Consequently, such codes may accurately reproduce the observed stellar spectrum, but do so with parameters that may be different from the true stellar properties. Spectral synthesis techniques begin to suffer dramatically for stars having spectral type K4 and later ($T_{\rm eff} \lesssim 4700$ K), due to the large number of atomic and molecular lines combined with missing or inaccurate values in the input line lists and associated quantum mechanical properties.

With this background in mind, we present a new method, "Empirical SpecMatch" (SpecMatch-Emp), for precision stellar characterization based on the direct comparison of observed optical spectra to a dense spectral library of touchstone stars with well-measured properties. A chief goal of SpecMatch-Emp is accuracy across the H–R diagram with a specific focus on stars of mid-K spectral type and later, due to the uncertainties associated with synthetic spectral techniques.

SpecMatch-Emp builds on a long history of stellar classification in astronomy using optical spectra. Founding work took place at the Harvard College Observatory (c. 1885–1925) with the visionary and heroic efforts of A. J. Cannon, A. P. Draper, and E. C. Pickering, which culminated in the HD catalog and the OBAFGKM classification sequence. A significant refinement by Morgan et al. (1943) included luminosity classes as an essential second dimension in the sequence (Gray & Corbally 2009).

SpecMatch-Emp extends this methodology by considering a third dimension, metallicity, and by returning numerical measurements of $T_{\rm eff}$, $R_\star$, and [Fe/H] of stellar parameters as opposed to categorical spectral classifications. This approach is enabled by the large and homogeneous sample of high-resolution spectra with high signal-to-noise ratio (S/N) gathered by the California Planet Search as part of its radial velocity programs to study extrasolar planets and by recent work to compile catalogs of touchstone stars with well-measured properties.

SpecMatch-Emp consists of two major parts: a spectral library and an algorithm for parameter measurement. In Section 2, we describe the construction of the spectral library of stars having properties determined by asteroseismology, interferometry, spectroscopy, and spectrophotometry. To address the scarcity of suitable mid- to late-K dwarfs in the literature, we present new precision measurements of 23 K dwarfs incorporating spectroscopy, SED modeling, and parallax measurements. This library of spectra and stellar parameters is publicly available for download as a monolithic memory-efficient file in Hierarchical Data Format (HDF5)[4] or as individual Flexible Image Transport System (FITS) files for each spectrum.[5]

In Section 3, we describe the SpecMatch-Emp algorithm, which compares an unlabelled target spectrum with the spectral library. The code, as well as easy-to-use command-line scripts, can also be obtained online.[6] In Section 4, we assess the accuracy of SpecMatch-Emp by performing an internal cross-validation analysis. We verified that for stars ranging from $T_{\rm eff} \approx 3000$–7000 K, SpecMatch-Emp yields $T_{\rm eff}$, $R_\star$, and [Fe/H] accurate to 100 K, 15%, and 0.09 dex respectively. We also investigate the performance of the algorithm at decreased S/N and spectral resolution by degrading the target spectra. We find that SpecMatch-Emp remains robust even at S/N as low as 10/pixel, as well as spectral resolutions down to about $R = 20{,}000$.

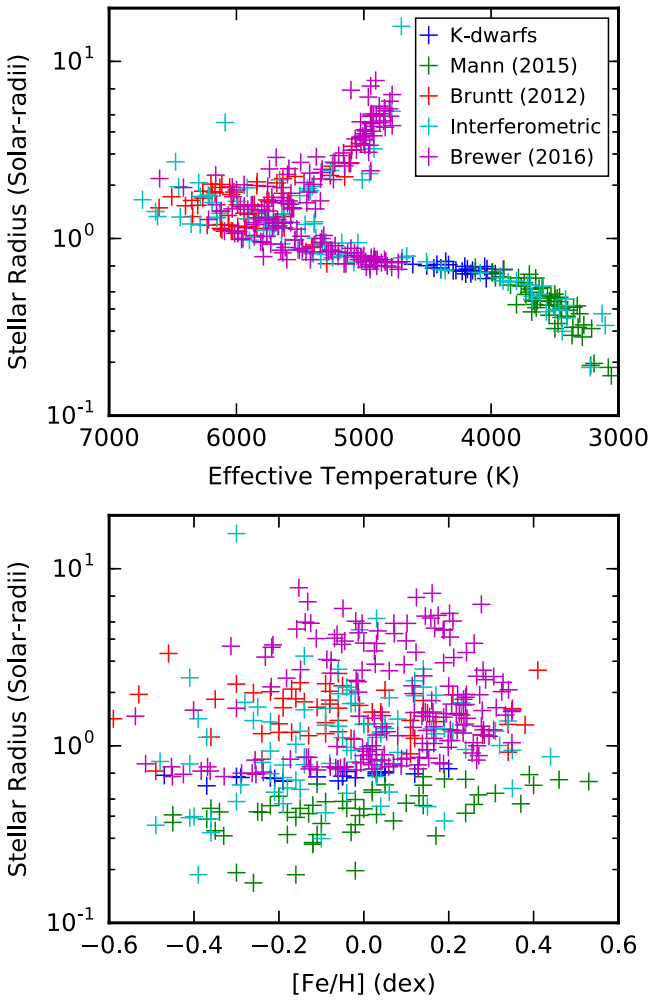

Figure 1. Distribution of SpecMatch-Emp library stars. The library covers the parameter space of $T_{\rm eff} \approx 3000$–7000 K, $R_\star \approx 0.16$–$16\,R_\odot$, [Fe/H] ≈ -0.5 to $+0.5$ dex. We have excluded stars having measured $v \sin i > 8.0$ km s^{-1} because their spectra retain insufficient information for the matching process.

2. Library

A crucial component of SpecMatch-Emp is the spectral library of 404 stars (see the Appendix), each with well-determined stellar parameters ($M_\star$, $R_\star$, $T_{\rm eff}$, [Fe/H]). As no single technique yields the best parameters across the H–R diagram, we have compiled the parameters for the stars in our library from a variety of different sources. By construction, our library contains stars that span a large region of the H–R diagram ($T_{\rm eff} \approx 3000$–7000 K, $R_\star \approx 0.1$–$16\,R_\odot$). The domain of $T_{\rm eff}$, $R_\star$, and [Fe/H] is shown in Figure 1 along with the provenance of the library parameters. We describe the source catalogs for these parameters in brief in Section 2.1. We augment this sample with new K-dwarf library stars in Section 2.2. In Section 2.3, we describe our conversion of the measured stellar properties into a homogeneous suite of

[4] https://zenodo.org/record/168084/files/library.h5
[5] http://web.gps.caltech.edu/~syee/hires_spectra/
[6] https://github.com/samuelyeewl/specmatch-emp

$T_{\rm eff}$, $\log g$, [Fe/H], $M_\star$, $R_\star$, and age measurements for each star. The details of the spectral data set are described in Section 2.4.

2.1. Library Parameters

2.1.1. Interferometric Sample

The library includes 95 stars having interferometrically determined radii with quoted uncertainties in radius of <5% compiled by von Braun et al. (2014).[7] This set of interferometric stars is the only sample included in our library to span the entire H–R diagram, because the other techniques face limitations in different regions of the parameter space. However, the relatively small number of stars with interferometric measurements necessitated the inclusion of stars from other sources.

2.1.2. Mann et al. (2015)

Mann et al. (2015) measured fundamental properties of 183 late-K and M dwarfs by performing an absolute flux calibration on optical and NIR spectra using literature photometry. The photometric measurements were calibrated with the updated filter profiles from Mann & von Braun (2015). The bolometric flux ($F_{\rm bol}$) was calculated by integrating over the flux-calibrated spectra, while $T_{\rm eff}$ was obtained by comparing the spectra with PHOENIX stellar atmosphere models. $F_{\rm bol}$ and $T_{\rm eff}$ were then combined with distance, d, measured by trigonometric parallax, to obtain the physical radius of the star ($R_\star$) using the Stefan–Boltzmann law:

$$L_\star = 4\pi d^2 F_{\rm bol} = 4\pi R_\star^2 \sigma T_{\rm eff}^4.$$

The analysis used empirical relations between spectral feature widths and [Fe/H] from Mann et al. (2013, 2014) to obtain the stellar metallicities. $M_\star$ was determined using empirical mass–luminosity relations from Delfosse et al. (2000). Both of these empirical relationships have been calibrated for M dwarfs. Median uncertainties for the stellar properties were 60 K in $T_{\rm eff}$, 3.8% in $R_\star$, 0.08 dex in [Fe/H], and 10% in $M_\star$. Our library includes 56 of the stars from this sample, for which we had suitable HIRES spectra. These comprise the majority of the M dwarfs in our library.

2.1.3. Brewer et al. (2016)

Brewer et al. (2016) conducted a detailed spectroscopic analysis of 1617 dwarf and subgiant stars with $T_{\rm eff}$ = 4700–6800 K observed by Keck/HIRES. Brewer et al. (2016) modeled the spectra with the spectral synthesis code SME (Valenti & Piskunov 1996), which has recently been updated to include many more lines (Brewer et al. 2015). We chose 177 of the stars from this analysis for our library, excluding stars with $v \sin i > 8$ km s^{-1}, S/N < 120/pixel, and [Fe/H] < −1.0 dex. We adopted the following uncertainties for the stellar parameters: 60 K in $T_{\rm eff}$, 0.05 dex in $\log g$, and 0.05 dex in [Fe/H] based on the comparisons with other independent techniques performed in Brewer et al. (2015, 2016).

[7] The compilation of von Braun et al. (2014) included results from Kervella et al. (2003), Baines et al. (2008, 2009), van Belle & von Braun (2009), von Braun et al. (2011a, 2011b, 2012), Boyajian et al. (2013), and Henry et al. (2013).

2.1.4. Bruntt et al. (2012)

Bruntt et al. (2012) examined 93 solar-type stars observed by *Kepler*, combining asteroseismology and spectroscopy to measure $T_{\rm eff}$, $\log g$, and [Fe/H]. The quoted uncertainties on these properties were 0.03 dex in $\log g$, 60 K in $T_{\rm eff}$, and 0.06 dex in [Fe/H]. We included 55 stars from this sample with HIRES spectra in our library.

2.2. K Dwarfs

Finding well-characterized mid- to late-K dwarfs (K4–K7; $T_{\rm eff} \approx 4700$–4000 K) proved to be particularly challenging. Detailed spectral synthesis codes such as SME and MOOG are challenged by the proliferation of deep metallic lines and the onset of MgH and TiO bands (Gray & Corbally 2009). Meanwhile, the empirical relations used in Mann et al. (2015) have not been calibrated for spectral types earlier than K7 ($T_{\rm eff} \lesssim 4100$ K). While measurements based on CHARA interferometry exist for a few such stars, coverage is sparse due to the small number of stars that are both bright enough at optical wavelengths and close enough for precise measurements of radius.

Due to the paucity of touchstone stars in the literature, we derived $T_{\rm eff}$ and $R_\star$ for 23 K4–K7 dwarfs using broadband photometry and constraints from parallax, $\pi_\star$. We drew stars from a sample of 110 included in a survey of planets around late-K dwarfs (Gaidos et al. 2013). After a search of literature photometry, we restricted this sample to the 23 stars having at least one literature measurement in the *UBVRIJHK* bands, which provide good coverage across the stellar SED.

We derived $T_{\rm eff}$ using an empirical $V - K$ color–temperature relationship from Boyajian et al. (2013):

$$T_{\rm eff} = a_0 + a_1(V-K) + a_2(V-K)^2 + a_3(V-K)^3$$

where

$$\begin{aligned} a_0 &= 8649 \pm 28 \text{ K} \\ a_1 &= -2503 \pm 35 \text{ K mag}^{-1} \\ a_2 &= 442 \pm 12 \text{ K mag}^{-2} \\ a_3 &= -31.7 \pm 1.5 \text{ K mag}^{-3}. \end{aligned}$$

The coefficients a_i are found in Table 8 of Boyajian et al. (2013) and were calibrated to 125 FGK stars with literature photometry and effective temperatures. Using this relation with existing literature photometry for our sample of K dwarfs, we were able to find $T_{\rm eff}$ to a typical uncertainty of ∼5%.

Next, we measured $F_{\rm bol}$ by fitting the broadband photometry with a stellar SED and integrating over wavelength. Our procedure for the SED fitting follows von Braun et al. (2014): we used the library of spectral templates from Pickles (1998) and fit them to literature photometry data via χ^2 minimization. We linearly interpolated between the published spectral templates to the nearest half spectral type to improve χ^2 fitting. For the literature photometry data, we make use of the modified filter profiles from Mann & von Braun (2015). Reddening is set to zero for all targets because of their small distances (<26 pc). After the template is scaled to minimize the reduced χ^2, bolometric flux is measured by integrating over wavelength.

21 stars from our sample have updated parallaxes from new *Gaia* data, as part of the Tycho–*Gaia* Astrometric Solution

Table 1
Properties of 23 K dwarfs

Name	HIP	V (mag)	K (mag)	$T_{\rm eff}$ (K)	$F_{\rm bol}$ (10^{-8} erg s^{-1} cm^{-2})	$\pi_\star$ (mas)	$R_\star$ ($R_\odot$)	[Fe/H] (dex)	Notes
GJ 1008.0	1532	9.92 ± 0.04	6.58 ± 0.03	4039 ± 241	0.66 ± 0.01	49.3 ± 0.4	0.59 ± 0.06	−0.37 ± 0.10	1
GJ 1044	10337	9.86 ± 0.04	6.54 ± 0.03	4051 ± 239	0.68 ± 0.01	42.6 ± 0.9	0.69 ± 0.07	0.12 ± 0.10	1
GJ 1127	47201	9.45 ± 0.03	6.37 ± 0.03	4207 ± 212	0.86 ± 0.01	44.5 ± 0.2	0.70 ± 0.05	0.03 ± 0.10	1
GJ 1172	66222	9.95 ± 0.04	6.38 ± 0.03	3904 ± 266	0.71 ± 0.01	48.8 ± 1.6	0.67 ± 0.09	−0.11 ± 0.10	2
GJ 3072	4845	10.03 ± 0.04	6.57 ± 0.06	3967 ± 301	0.62 ± 0.01	46.7 ± 0.4	0.63 ± 0.07	−0.19 ± 0.10	1
GJ 3494	40910	9.76 ± 0.04	6.61 ± 0.03	4159 ± 228	0.68 ± 0.01	44.3 ± 0.3	0.63 ± 0.05	−0.06 ± 0.10	1
GJ 9093	12493	9.52 ± 0.03	6.54 ± 0.03	4276 ± 193	0.74 ± 0.01	41.9 ± 0.3	0.66 ± 0.05	−0.29 ± 0.10	1
GJ 9144	19165	9.69 ± 0.03	6.74 ± 0.03	4298 ± 200	0.64 ± 0.01	38.7 ± 0.2	0.66 ± 0.05	−0.22 ± 0.10	1
HD 178126	93871	9.22 ± 0.02	6.47 ± 0.03	4449 ± 177	0.87 ± 0.01	40.8 ± 0.3	0.68 ± 0.04	−0.47 ± 0.10	1
HD 200779	104092	8.30 ± 0.02	5.33 ± 0.04	4283 ± 211	2.47 ± 0.01	66.6 ± 0.2	0.76 ± 0.06	0.07 ± 0.10	1
HD 20280	15095	9.16 ± 0.02	6.11 ± 0.03	4227 ± 199	1.14 ± 0.01	54.0 ± 0.3	0.65 ± 0.05	−0.21 ± 0.10	1
HD 203040	105341	9.10 ± 0.04	5.75 ± 0.03	4033 ± 242	1.38 ± 0.01	63.2 ± 0.5	0.67 ± 0.06	−0.05 ± 0.10	1
HD 218294	114156	9.62 ± 0.02	6.45 ± 0.03	4146 ± 209	0.75 ± 0.01	45.1 ± 0.3	0.66 ± 0.05	−0.02 ± 0.10	1
HD 224607	118261	8.70 ± 0.05	6.15 ± 0.03	4615 ± 214	1.29 ± 0.01	44.0 ± 0.2	0.71 ± 0.05	−0.04 ± 0.10	1
HD 35171	25220	7.94 ± 0.03	5.26 ± 0.03	4505 ± 179	2.74 ± 0.02	68.5 ± 0.3	0.70 ± 0.04	0.05 ± 0.10	1
HD 355784	97051	9.96 ± 0.05	6.87 ± 0.03	4200 ± 248	0.53 ± 0.01	38.5 ± 0.3	0.63 ± 0.06	−0.19 ± 0.10	1
HD 59582	36551	8.98 ± 0.03	6.16 ± 0.03	4395 ± 193	1.13 ± 0.01	48.5 ± 0.3	0.67 ± 0.05	−0.30 ± 0.10	1
HD 68834	40375	8.82 ± 0.04	5.92 ± 0.03	4334 ± 209	1.39 ± 0.01	52.0 ± 0.3	0.71 ± 0.05	0.03 ± 0.10	1
HD 7279	5663	9.56 ± 0.04	6.45 ± 0.03	4186 ± 222	0.77 ± 0.01	44.0 ± 0.3	0.67 ± 0.06	−0.05 ± 0.10	1
HD 80632	45839	9.10 ± 0.04	6.32 ± 0.03	4426 ± 198	0.99 ± 0.01	41.8 ± 0.2	0.71 ± 0.05	0.05 ± 0.10	1
HD 85488	48411	8.85 ± 0.03	5.98 ± 0.03	4357 ± 199	1.30 ± 0.01	47.7 ± 1.5	0.74 ± 0.07	0.20 ± 0.10	2
HD 97214	54651	9.23 ± 0.03	6.36 ± 0.03	4357 ± 197	0.87 ± 0.01	50.5 ± 0.4	0.58 ± 0.04	−0.89 ± 0.10	1
HD 97503	54810	8.70 ± 0.02	5.88 ± 0.03	4395 ± 185	1.46 ± 0.01	54.2 ± 0.3	0.68 ± 0.04	0.03 ± 0.10	1

Note. Parameters of newly characterized K4–K7 dwarfs determined by combining an empirical color–temperature relation, SED fitting, and stellar parallaxes. 1: Parallax from the Tycho–*Gaia* Astrometric Solution (TGAS; Michalik et al. 2015; Gaia Collaboration et al. 2016; Lindegren et al. 2016). 2: Parallax from *Hipparcos*.

(This table is available in machine-readable form.)

(TGAS; Michalik et al. 2015; Gaia Collaboration et al. 2016; Lindegren et al. 2016). These stars have uncertainties in parallax, $\sigma(\pi_\star) \approx 0.3$ mas. For the remaining two stars (GJ 1172 and HD 85488), we used the parallax values calculated in the van Leeuwen reduction of *Hipparcos* data with $\sigma(\pi_\star) \approx 1.6$ mas (Perryman et al. 1997; van Leeuwen 2007). Combining $T_{\rm eff}$, $F_{\rm bol}$, $\pi_\star$, and the Stefan–Boltzmann law, we calculated $R_\star$. The median uncertainty in $R_\star$ over the entire sample was 7.4%, dominated primarily by the uncertainties in $T_{\rm eff}$ from the color–temperature relation.

Finally, we adopted the metallicity values found in Gaidos et al. (2013), which were derived using `SME` (Valenti & Piskunov 1996). While traditional spectroscopic techniques begin to suffer for $T_{\rm eff} \lesssim 4700$ K, they are the only source of metallicity measurements for this sample of K dwarfs. More accurate metallicities could be derived by observing K dwarfs with G dwarf companions, for which metallicity can be measured more accurately from spectral synthesis. Such a study is beyond the scope of this work. We adopt 0.1 dex as the uncertainty on [Fe/H] and note that such errors are likely systematic (rather than statistical) in nature. The final set of parameters used for these K dwarfs is listed in Table 1.

2.3. Isochrone Analysis

The catalogs of stars presented in Section 2.1 often do not list a complete set of $T_{\rm eff}$, $R_\star$, $M_\star$, $\log g$, and [Fe/H]. For example, the interferometric sample (Section 2.1.1) does not include measurements of $M_\star$. To obtain a homogeneous suite of parameters, we combine the known properties with the Dartmouth models (Dotter et al. 2008). We use the `isochrones` software package (Morton 2015), which performs a Markov chain Monte Carlo (MCMC) fit to estimate the remaining stellar parameters from the stellar model grid. To account for systematic errors in the Dartmouth models, we adopt the 5th and 95th percentiles of the final MCMC distribution as the parameter uncertainties.

2.4. Optical Spectra

The spectra were observed with the High Resolution Echelle Spectrometer (HIRES; Vogt et al. 1994) at the Keck-I 10 m telescope as part of the various programs of the California Planet Search (CPS) to study extrasolar planets. For information about CPS and its goals, see Howard et al. (2010). The spectra have a resolution $R \approx 60{,}000$. We selected stars with spectra having S/N of at least 40/pixel, with most (∼80%) having S/N of >100 per HIRES pixel on blaze near 550 nm.

The extracted spectra are from the middle chip of HIRES and contain 16 orders with 4021 intensity measurements per order. Each order is imprinted with the HIRES blaze function, which we remove by dividing the observed spectrum with a calibration spectrum constructed from several rapidly rotating B stars. Owing to different line-of-sight velocities, the library spectra are shifted with respect to one another in pixel coordinates. It is convenient to adopt a common wavelength scale and register each spectrum to this scale. We resampled our spectra onto a new wavelength scale ($\lambda = 4990$–6410 Å) that is uniform in $\Delta\log\lambda$. We then removed the shifts due to the stars' individual line-of-sight velocities by registering our spectra against the solar spectrum of the National Solar Observatory (NSO) (Kurucz et al. 1984) according to the procedure described in Section 3.1. The final library data set thus consists of a 404 × 73,788 array of normalized spectra on

the rest wavelength scale, together with associated stellar parameters.

3. SpecMatch-Emp

Here, we describe the SpecMatch-Emp algorithm. Given an unknown spectrum, SpecMatch-Emp first shifts it onto the library wavelength scale to correct for its individual radial velocity (Section 3.1). We then identify the most similar library spectra (Section 3.2) and interpolate between them (Section 3.3) to arrive at a final set of derived parameters for the target star.

We report $T_{\rm eff}$, $R_\star$, and [Fe/H] in contrast to most spectral analysis codes, which report $T_{\rm eff}$, $\log g$, and [Fe/H]. While $R_\star$ is closely related to $\log g$, it is the directly observed quantity for the library stars K4 and later. We could, in principle, derive $\log g$ values by appealing to stellar models, but such models have known systematic errors that are largest for cool stars. For example, in their study of M dwarfs, Mann et al. (2015) found that the Dartmouth models systematically overpredict stellar radii by ≈5%. Therefore, to mitigate systematic errors in the derived stellar radii of late-type stars, where SpecMatch-Emp performs best, we choose to parameterize stars in terms of $T_{\rm eff}$, $R_\star$, and [Fe/H].

3.1. Spectral Registration

We begin by resampling each of the 16 orders of the HIRES spectrum onto the library wavelength scale. Because the library wavelength scale is uniform in $\Delta\log\lambda$, fixed velocity shifts between the spectra correspond to a uniform displacement in the wavelength sampling. We also mask out the telluric lines due to atmospheric O_2 absorption in the wavelength region $\lambda = 6270$–6310 Å, because these lines are fixed in the observatory frame, not in the stellar rest frame.

Each masked order is then divided into segments of length ∼700 pixels, which are then cross-correlated with the reference spectrum. This operation is performed in Fourier space and low-frequency Fourier modes are filtered out such that only spectral lines, and not long-baseline differences in continuum normalization, contribute to the cross-correlation. For each segment, we find the ideal pixel shift by fitting a parabola to the cross-correlation peak. We fit a line through these shifts to obtain a linear relationship between the pixel shift and pixel number across each order (Figure 2). As an example of the results, we show the observed and registered spectrum of HD 190406 in Figure 3.

As a matter of convenience, all the library spectra are shifted onto a single wavelength scale, chosen to be that of the NSO solar spectrum. However, for stars with spectral types unlike the Sun, performing the cross-correlation against the NSO spectrum gives poor results, with multiple spurious peaks that do not correspond to the true velocity shift (see the left panel of Figure 4).

To address this, we use a bootstrapping approach in which four additional spectra belonging to stars of different spectral types were shifted successively onto the NSO wavelength scale, forming a ladder of template spectra. These additional spectra were chosen from our highest S/N spectra (S/N > 160/pixel), with roughly solar metallicities and spaced evenly in $T_{\rm eff}$ and $R_\star$. When presented with an unknown target spectrum, we find the best reference spectrum by performing the cross-correlation procedure described above on a single order of the target spectrum. The reference spectrum that gives the largest median cross-correlation peak with the target is deemed to have the greatest similarity to the target and is then used to shift the rest of the target spectrum. We selected the spectral order that spans $\lambda = 5120$–5210 Å as the benchmark order because of the rich spectral information contained in this region across all spectral types. In Figure 5, we illustrate the successful registration of Barnard's star (GL699, spectral type M4V) to the NSO scale with our bootstrapping approach.

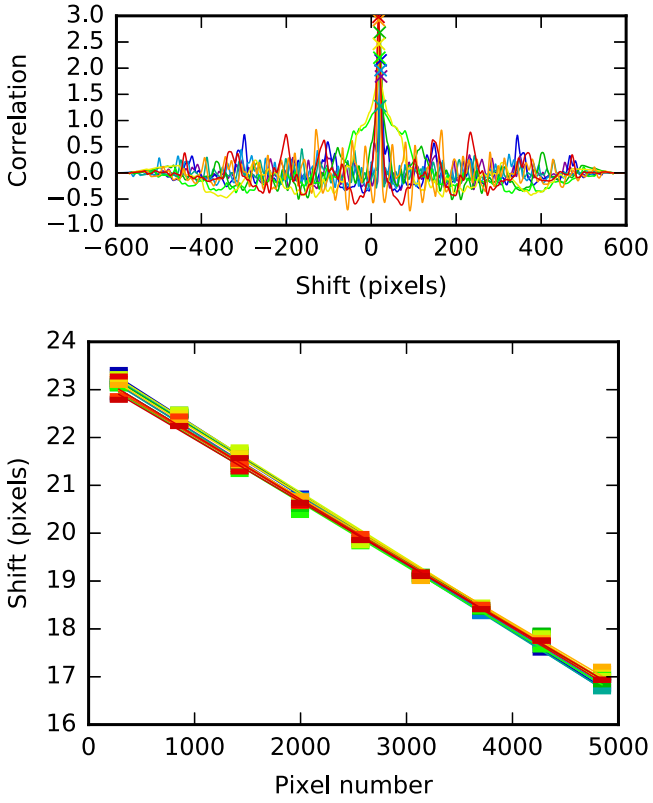

Figure 2. Registration of a solar-type spectrum using cross-correlation (see Section 3.1). Top: cross-correlation of a single order of the spectrum of HD 190406 (spectral type G0V) with corresponding regions of the solar spectrum. Each line corresponds to a particular segment. The maximum correlation for each segment is indicated with a cross. Bottom: the shifts calculated for the various segments of each order are fit with a first-order polynomial, which is then applied to shift the corresponding pixels. Outliers result from poor cross-correlation results in that region of the spectrum and are clipped before the fit is performed.

3.2. Matching

Once the target spectrum has been shifted and flattened onto the library wavelength scale, we compare it to each of the library spectra, in segments of 100 Å (see Table 2). In each comparison, we first modify the library spectrum by applying a rotational broadening kernel (Equation (17.12) in Gray 1992) to account for the relative $v \sin i$ between the target and reference stars. We found that it was necessary to set an upper limit on relative $v \sin i$, chosen to be 10 km s^{-1}, to prevent the reference spectrum from being broadened excessively. If the kernel was allowed to go to arbitrarily high $v \sin i$ values, it would allow seemingly better matches even with dissimilar spectra as a result of the loss of spectral information from broadening. We also fit a cubic spline through the residuals between the target and reference spectra, using knots placed at

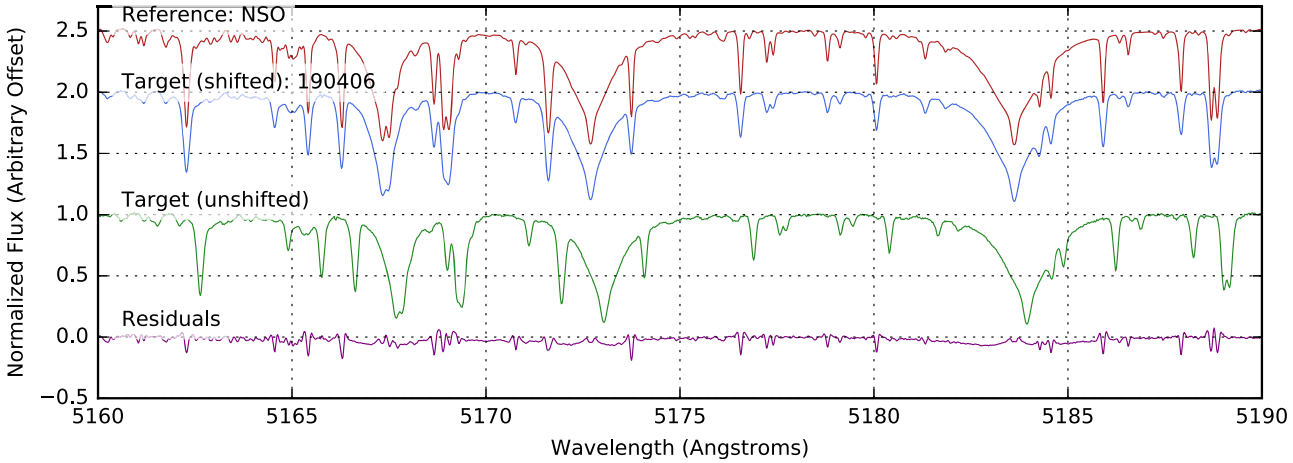

Figure 3. Solar reference spectrum and spectrum of HD 190406 (spectral type G0V) before and after registration (see Section 3.1).

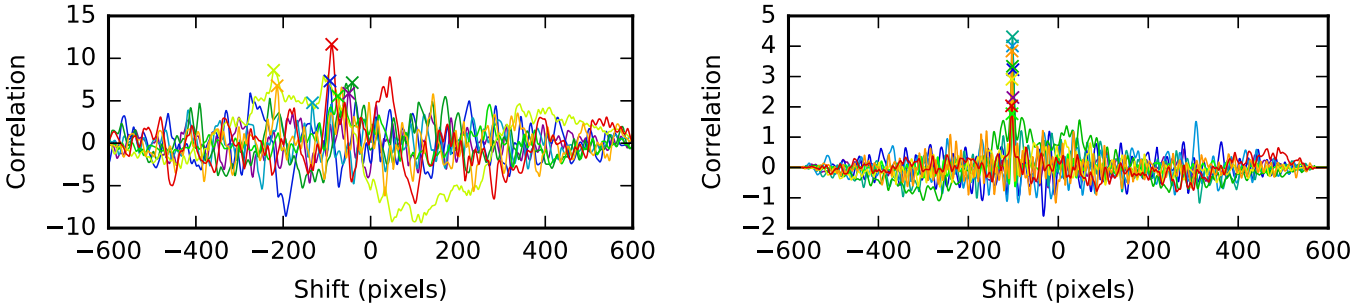

Figure 4. Cross-correlation of the different segments in a single order of the spectrum of Barnard's star (GL669, spectral type M4V), against the solar spectrum (left) and an M dwarf spectrum (right). Due to the dissimilarity in spectra, the cross-correlation with the solar spectrum gives multiple peaks that do not correspond to the true shift, whereas the previously shifted M dwarf spectrum serves as a better reference (see Section 3.1).

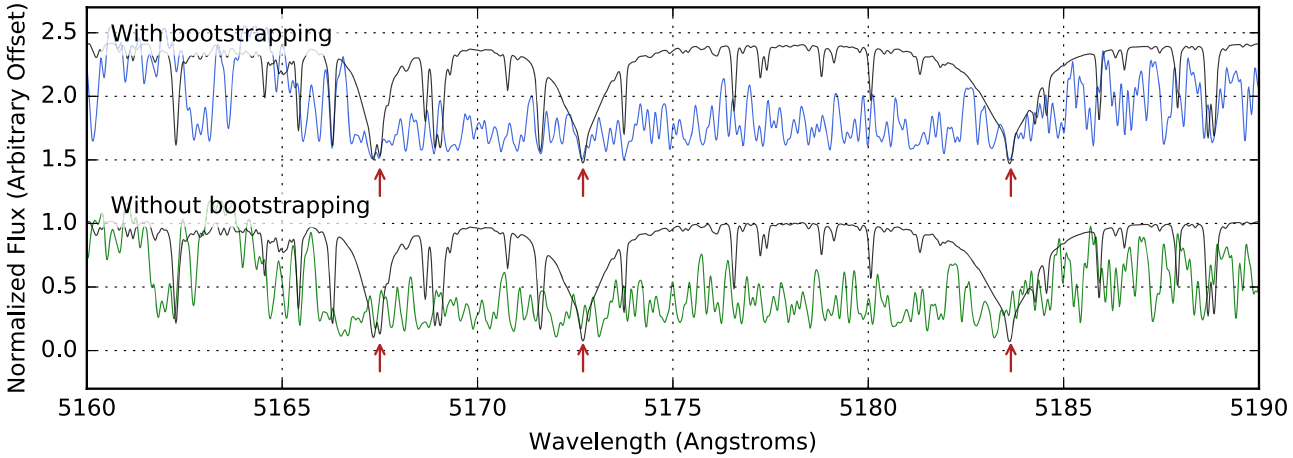

Figure 5. Spectrum of Barnard's star (GL699, spectral type M4V) when shifted against the solar spectrum (bottom) and against a previously shifted template M dwarf spectrum (top). The solar spectrum, which was chosen to be the library rest wavelength scale, is overlaid in gray. Red arrows indicate specific spectral features that are properly aligned only when the target spectrum is shifted against the M dwarf reference. We achieve superior spectral registration by using the bootstrapping approach described in Section 3.1 to derive a ladder of wavelength standards of different spectral types.

20 Å intervals. Subtracting this spline amounts to using a high-pass filter, which ensures that the χ^2 is not influenced by slowly varying ($\gtrsim$20 Å) residual structure due to imperfections in the removal of the blaze function.

We adopt the unnormalized χ^2 statistic as the figure of merit that quantifies the degree of similarity between the target and modified reference spectra:

$$\chi^2 = \sum (s_{\rm ref} - s_{\rm target})^2.$$

The pixel-by-pixel Poisson uncertainties are not included because the main residual differences in the spectra are due

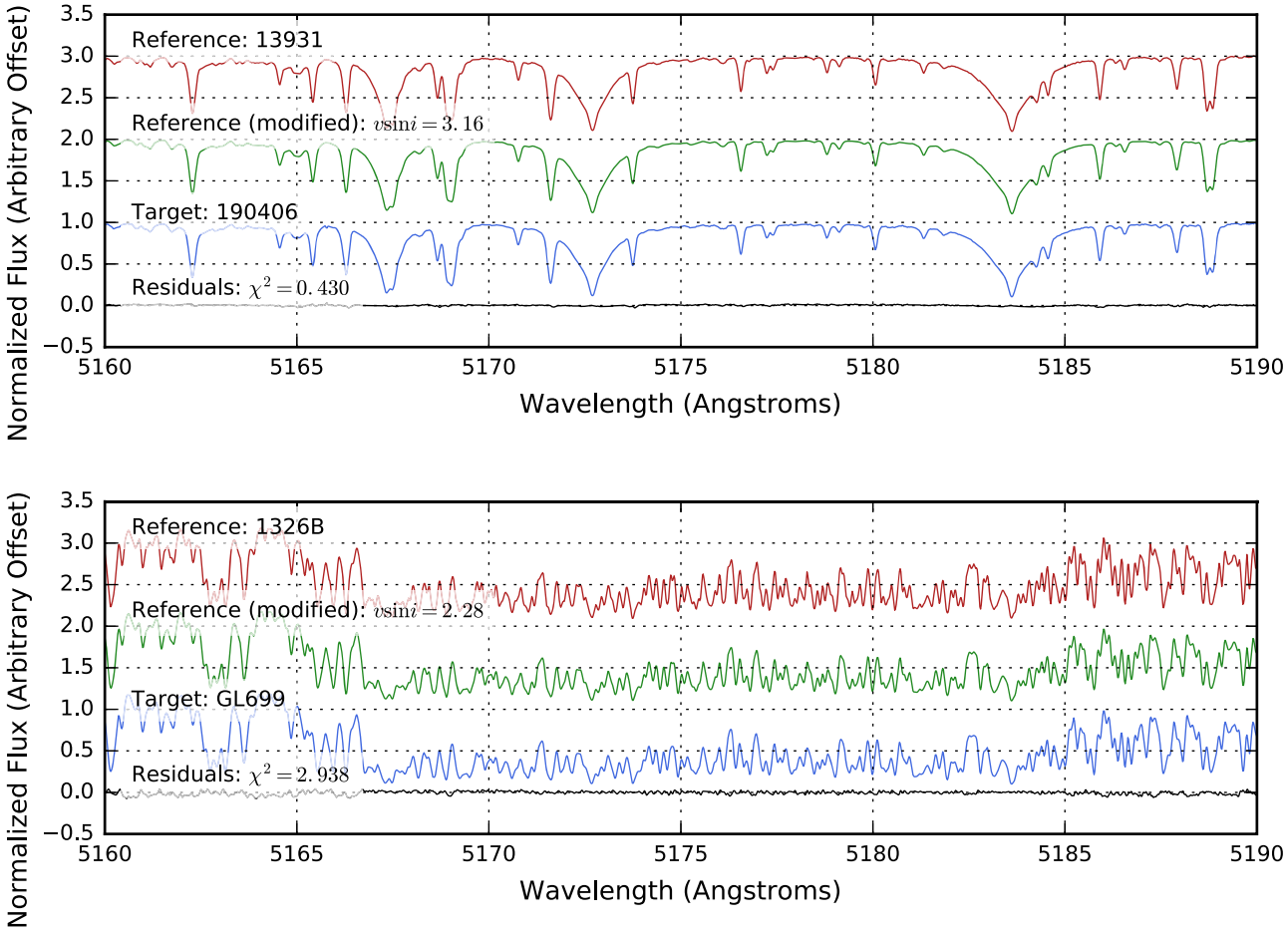

Figure 6. Best-matching library spectra to HD 190406 (top) and GL699 (bottom). The modified reference spectra are the library spectra after applying a broadening kernel and fitting a cubic spline to the continuum (see Section 3.2).

Table 2
Wavelength Regions used in Both the Matching and Linear Combination Steps in `SpecMatch-Emp`

Region	Wavelength Range
1	5000–5100 Å
2	5100–5200 Å
3	5200–5300 Å
4	5300–5400 Å
5	5400–5500 Å
6	5500–5600 Å
7	5600–5700 Å
8	5700–5800 Å

to astrophysical differences, not photon noise. Including photon errors would give lower χ^2 values when comparing with library spectra with poorer S/N, even if these spectra are dissimilar to the target. We verify in Section 4.2 that `SpecMatch-Emp` is dominated by systematics, not photon statistics down to S/N of 10/pixel.

Allowing for $v \sin i$ and continuum normalization to float as free parameters, we use a nonlinear least-squares minimization package `lmfit` (Newville et al. 2014) to minimize χ^2, finding the best possible match between the target and reference spectra. We then repeat this matching process over all the library spectra, recording in each case the lowest χ^2 value achieved. We illustrate the results of the matching step for HD 190406, a solar-type star, and Barnard's star (GL699), an M4V star, in Figures 6 and 7. Figure 6 shows the best-matching spectra from the library and Figure 7 shows the distribution of χ^2.

3.3. Linear Combination

The `SpecMatch-Emp` routine then interpolates between the parameters of the library spectra by synthesizing linear combinations of the five best-matching spectra as found in the previous step. We form a new composite spectrum, $S_{\rm lc} = \sum_{i=1}^{5} c_i S_i$, where each spectrum, S_i, is broadened by the optimal $v \sin i$ found in the previous matching stage. We chose to use five spectra in these linear combinations by trial and error. We use `lmfit` to find the set of coefficients $\{c_1, c_2, ..., c_5\}$ that minimizes χ^2 when compared with the target spectrum. The c_i's are subject to the constraint that they should sum to unity by incorporating a narrow Gaussian prior of width $\sigma = 10^{-3}$, such that:

$$\chi^2 = \sum (s_{\rm lc} - s_{\rm target})^2 + \left(\sum c_i - 1\right)^2 / 2\sigma^2.$$

In this step, we continue to correct for differences in continuum normalization by fitting a cubic spline and allowing the spline parameters to float as we minimize χ^2.

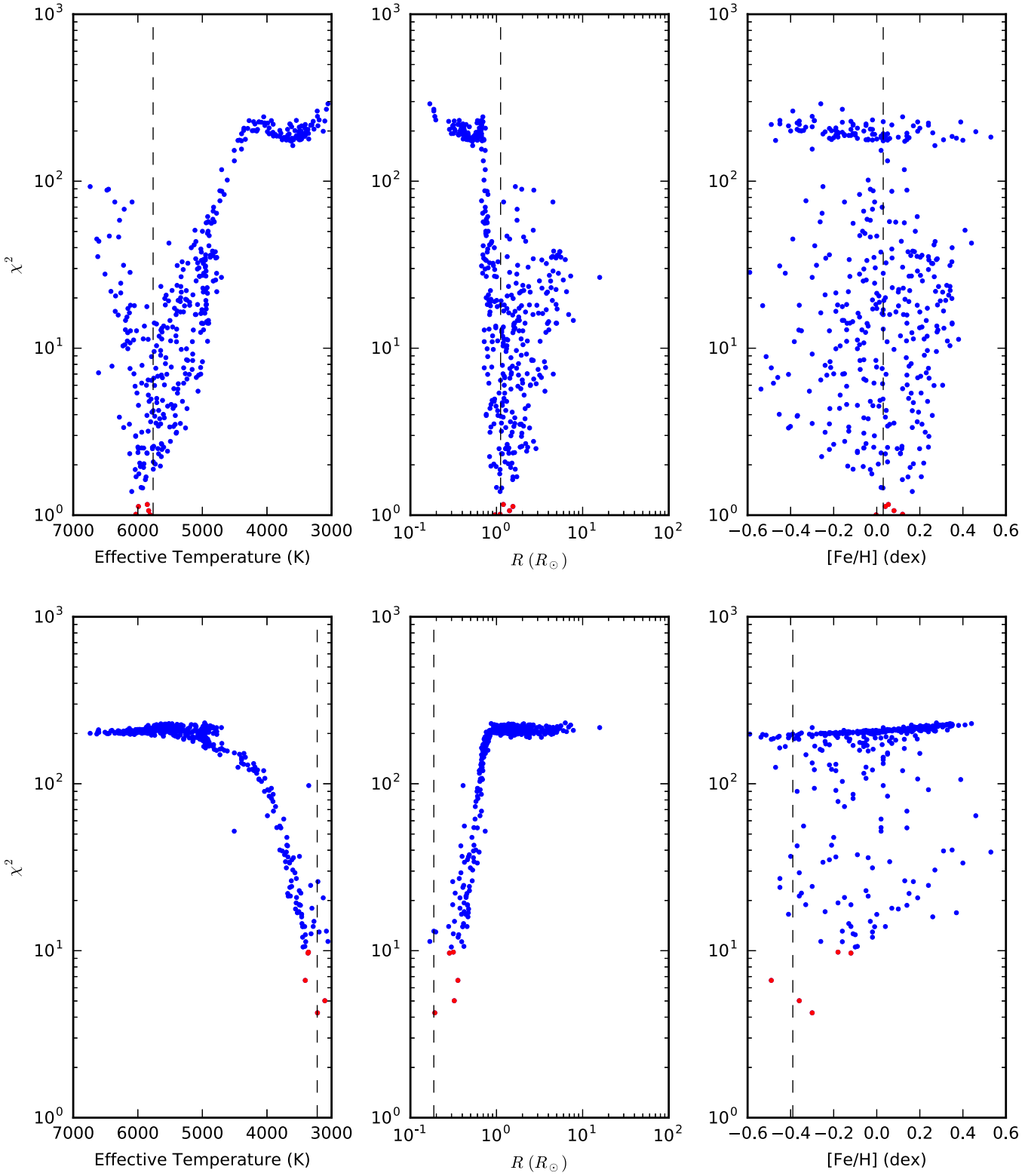

Figure 7. Best chi-squared values for the matches between the spectrum of HD 190406 (top) and GL699 (bottom) with each library spectrum, plotted against the library star parameters (see Section 3.2). The stars with the five lowest chi-squared values are displayed in red, and we see that there is a sharp minimum in chi-squared close to the true target parameters, indicated by the vertical line. This match was performed in the wavelength region 5300–5400 Å.

We thus obtain a new spectrum that matches the target spectrum even more closely than any individual library spectrum. We show example results in Figures 8 and 9.

The set of coefficients c_i found that minimizes χ^2 is then used to create a weighted average of the parameters of the reference stars. In order to incorporate the spectral

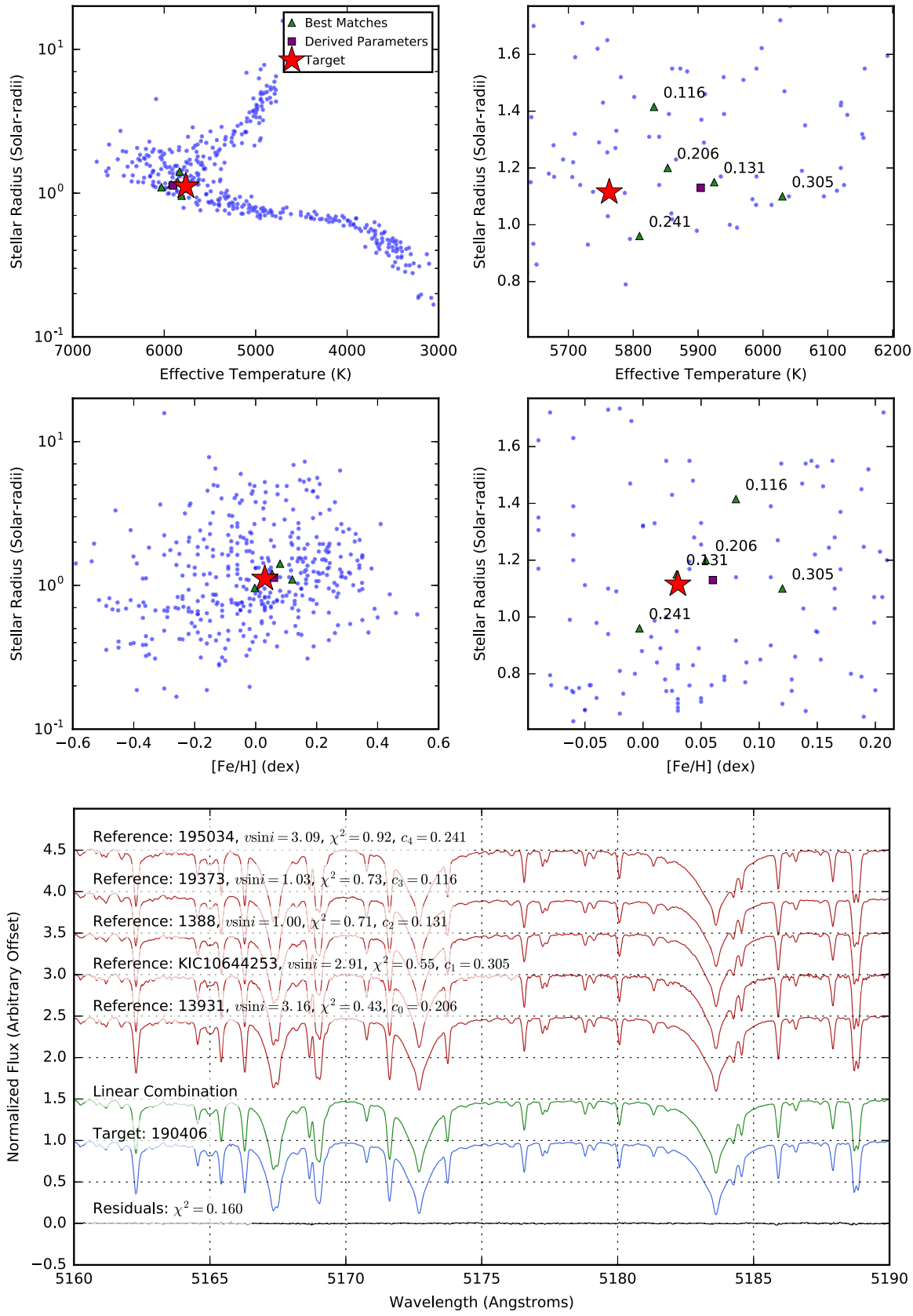

Figure 8. Results from the linear combination approach (Section 3.3) for the star HD 190406. Top: the position of the five reference stars used, with their respective coefficients. The star indicates the library parameters of the target, while the purple square denotes the weighted average of the reference parameters. Bottom: the reference spectra and linear combination found. The final χ^2 of 0.160 for the linear combination is lower than the χ^2 for the best-matching single spectrum, $\chi^2 = 0.43$.

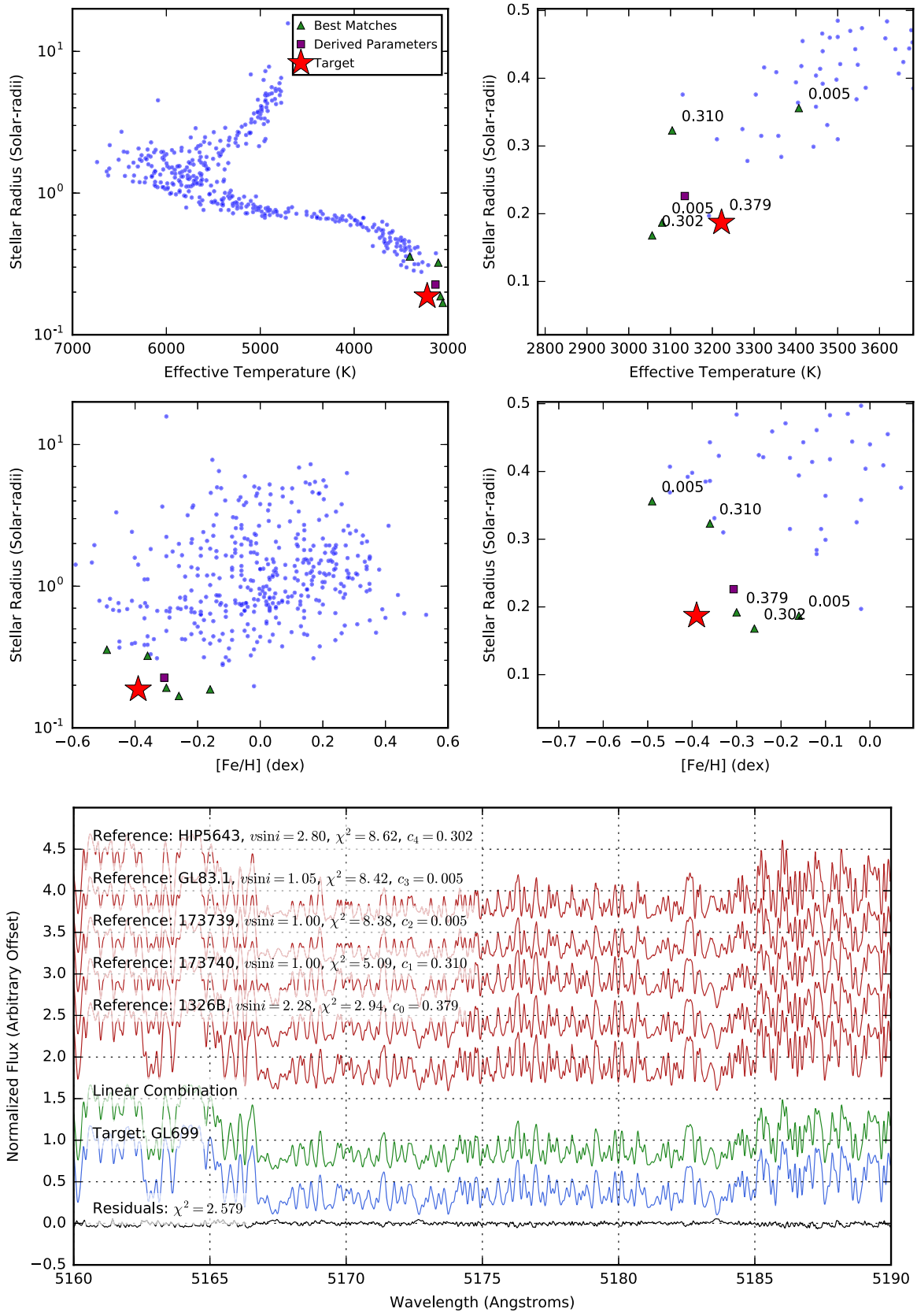

Figure 9. Same as Figure 8, but for the star GL699. The final residuals between the target star and the linear combination vanish almost completely (see Section 3.3).

information from the entire spectrum, we average the derived parameters from each 100 Å segment to obtain a final set of stellar parameters for the target. In total, it takes approximately 10 minutes to obtain the final parameters from a raw, unshifted spectrum on a modern (c. 2016) desktop computer.

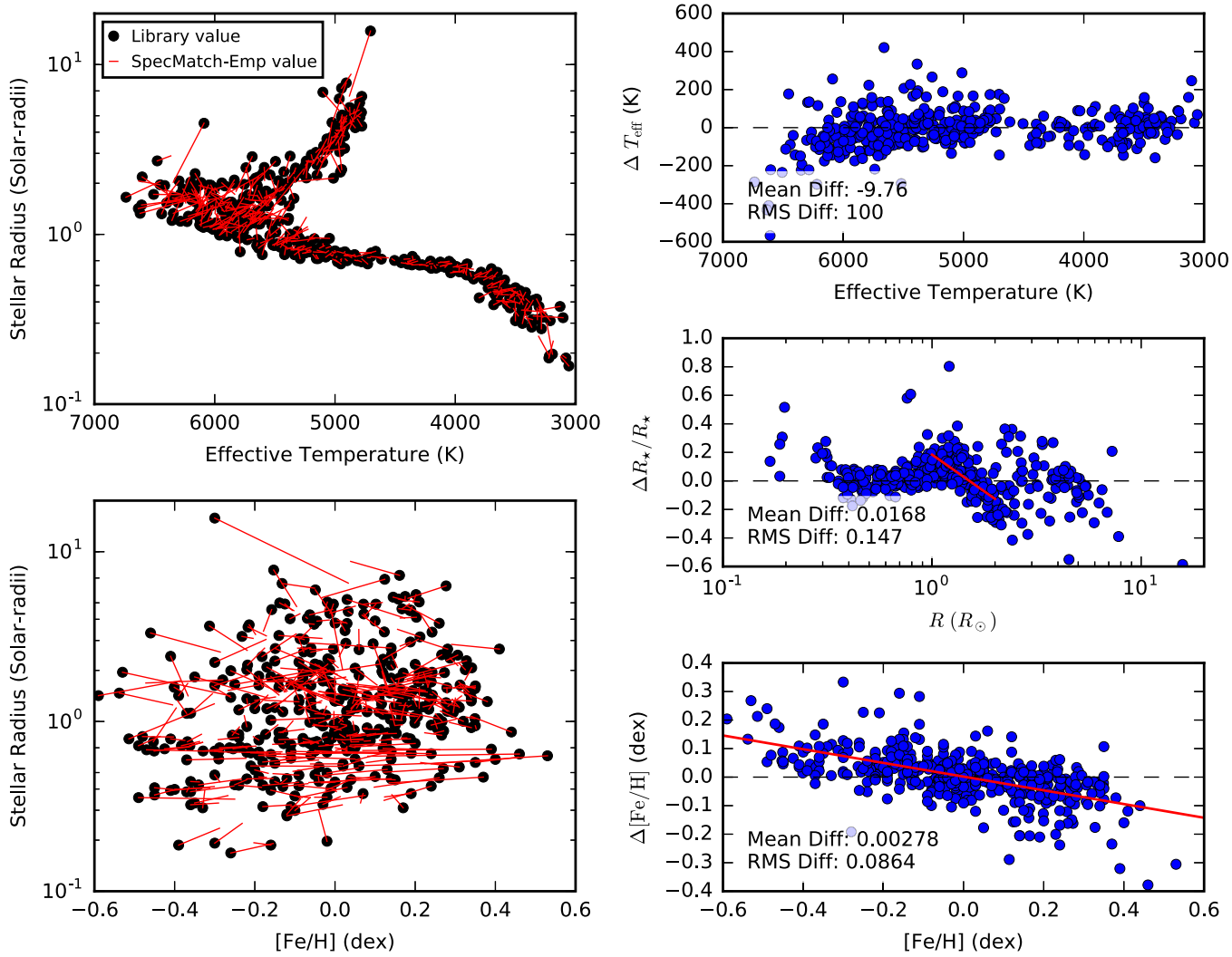

Figure 10. Comparison of library parameters to parameters derived from SpecMatch-Emp for each library spectrum in the validation process (Section 4.1). Left: black points indicate the library stellar parameters, while red lines point to the SpecMatch-Emp parameters. Right: differences between the library values of $T_{\rm eff}$, $R_\star$, [Fe/H], and the derived values. The red lines show the trends in the residuals, which we attempt to fit.

4. Performance

4.1. Accuracy

To assess the accuracy of `SpecMatch-Emp`, we performed an internal cross-validation, where we treated each star in the library as an unknown target and ran `SpecMatch-Emp` to compute its parameters from the remaining library spectra. We then compared these derived parameters to their library values. The difference between the derived parameters and the library parameters reflects the errors in the `SpecMatch-Emp` algorithm and in the library parameters.

Figure 10 shows the results of this validation process. We notice a general tendency for the residuals to be most negative for larger values of the derived parameter, and most positive for smaller values. This can be partly explained by the fact that our library spectra are not on an infinite grid, but occupy only a finite region of parameter space. Target stars must necessarily match stars in the interior of that space, resulting in their derived parameters being pulled toward the interior of the distribution. On the one hand, this effect amounts to a source of systematic uncertainty resulting from the use of real spectra of nearby stars, as opposed to using model spectra that can be synthesized with arbitrary properties. On the other hand, `SpecMatch-Emp` guards against returning combinations of parameters that are not realized among nearby stars, whereas spectral synthesis may wander into unphysical parameter space.

We attempt to mitigate the effect of regression toward the mean by recalibrating the derived parameters. The effect is most pronounced for the residuals in [Fe/H], and we fit a first-order polynomial to the residuals, obtaining the following correction:

$$[{\rm Fe/H}]_{\rm cal} = 1.240\,[{\rm Fe/H}]_{\rm SM} - 0.0018. \quad (1)$$

We perform a similar detrending for $R_\star$, but restrict the fit to derived parameters of $1.0 < R_\star/R_\odot < 2.0$, where the effect is most pronounced. For other values of $R_\star$, the library stars are restricted to a narrow region of the H–R diagram, so the derived parameters are also confined to a narrow range. However, the main sequence is relatively broad for stars with $T_{\rm eff} > 5500$ K and $R_\star = 1$–$2\ R_\odot$, so we see a larger spread of derived $R_\star$ values and the effect of regression to the mean is more pronounced.

The empirical relation we used to recalibrate the derived radii is given in Equation (2). In this case, the calibration

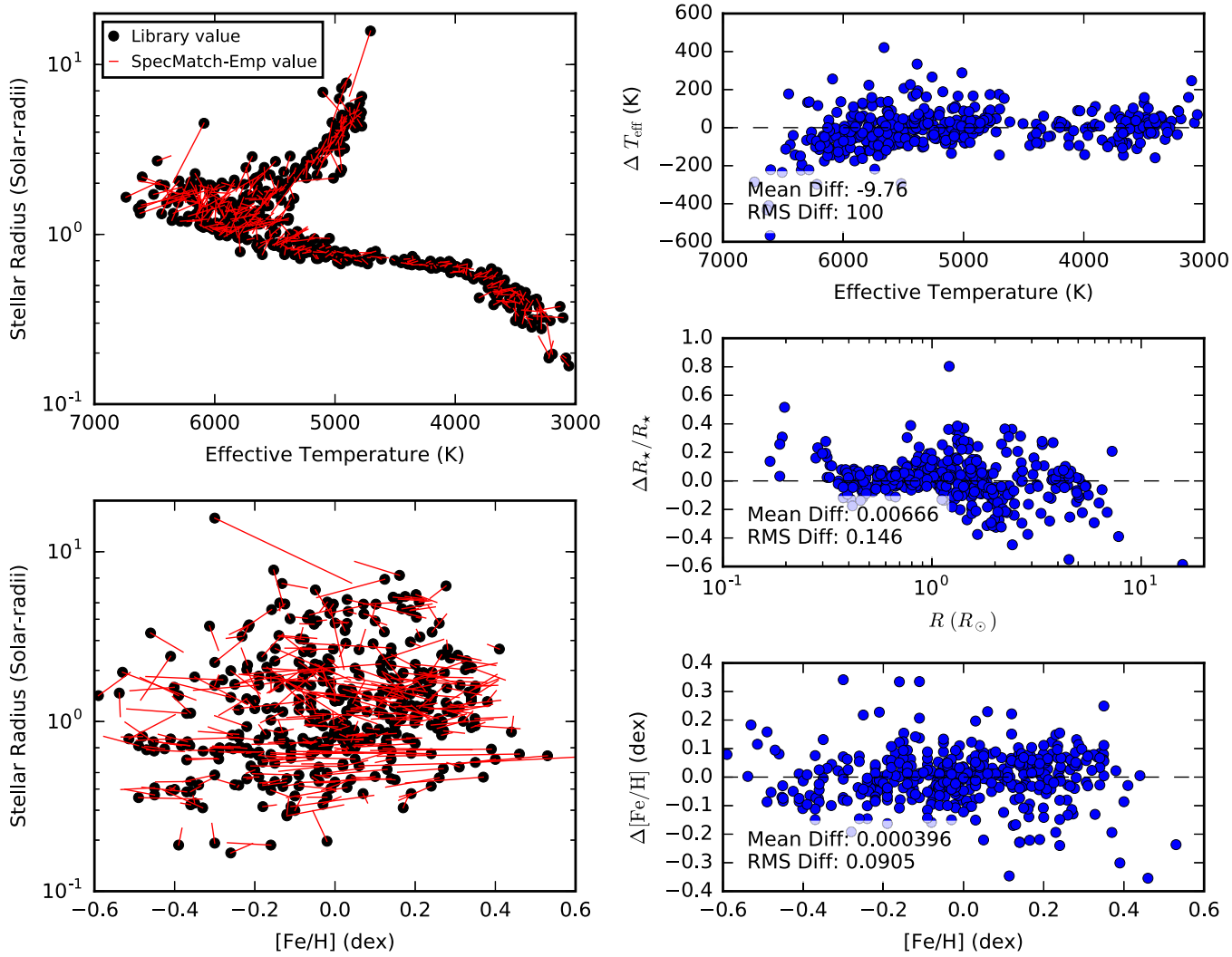

Figure 11. Same as 10, but after performing detrending (see Section 4.1).

Table 3
rms Difference between Library Parameters and Those Derived from SpecMatch-Emp for Each Star

	$\sigma(T_{\rm eff})$ (K)	$\sigma(\Delta R_\star/R_\star)$	σ([Fe/H]) (dex)
All stars	100	0.15	0.09
$T_{\rm eff} < 4500$ K	70	0.10	0.12
$T_{\rm eff} \geqslant 4500$ K	110	0.16	0.08

Note. Different uncertainties may be adopted for stars from different regions of the H–E diagram, because the accuracy of SpecMatch-Emp depends on the distribution of library stars in that region as well as the scatter of the library parameters for those stars.

relation is quadratic, because we are fitting a trend in $\Delta R/R$:

$$R_{\star,\rm cal} = 0.560R^2_{\star,\rm SM} + 0.165R_{\star,\rm SM}. \quad (2)$$

The final, detrended results are shown in Figure 11. For all our library stars, the differences between the derived and library values had a scatter of 100 K in $T_{\rm eff}$, 15% in $R_\star$, and 0.09 dex in [Fe/H]. These values, listed in Table 3, are the uncertainties that should be adopted for the output of SpecMatch-Emp.

When restricting our analysis to the cool stars (Figure 12), with $T_{\rm eff} < 4500$ K, the performance of SpecMatch-Emp improves to 70 K in $T_{\rm eff}$, 10% in $R_\star$, and 0.12 dex in [Fe/H]. For cool stars, most of the stars are from the sample of Mann et al. (2015), which has a median uncertainty of 60 K in $T_{\rm eff}$, 4% in $R_\star$, and 0.08 dex in [Fe/H]. In this region then, the accuracy of SpecMatch-Emp of the routine appears to be primarily limited by the uncertainties in the library parameters, which set the theoretical limit on accuracy.

4.2. Performance at Low S/N

We also investigated the effect of photon shot noise on the precision of the parameters derived from SpecMatch-Emp. We chose a subset of 22 stars from the library, distributed across the H–R diagram and with original S/N > 160/pixel. Their unshifted spectra are then degraded to lower S/N by injecting Gaussian noise into the raw spectra. We chose target S/Ns of 120, 80, 40, 20, and 10 per HIRES pixel. For each target spectrum and S/N level we generated 20 noisy spectra. We then analyzed these spectra through the SpecMatch-Emp routine and compared the final properties to those derived from the original high-S/N spectra.

Figure 13 shows the rms difference between the noisy derived parameters and the high-S/N derived parameter, for

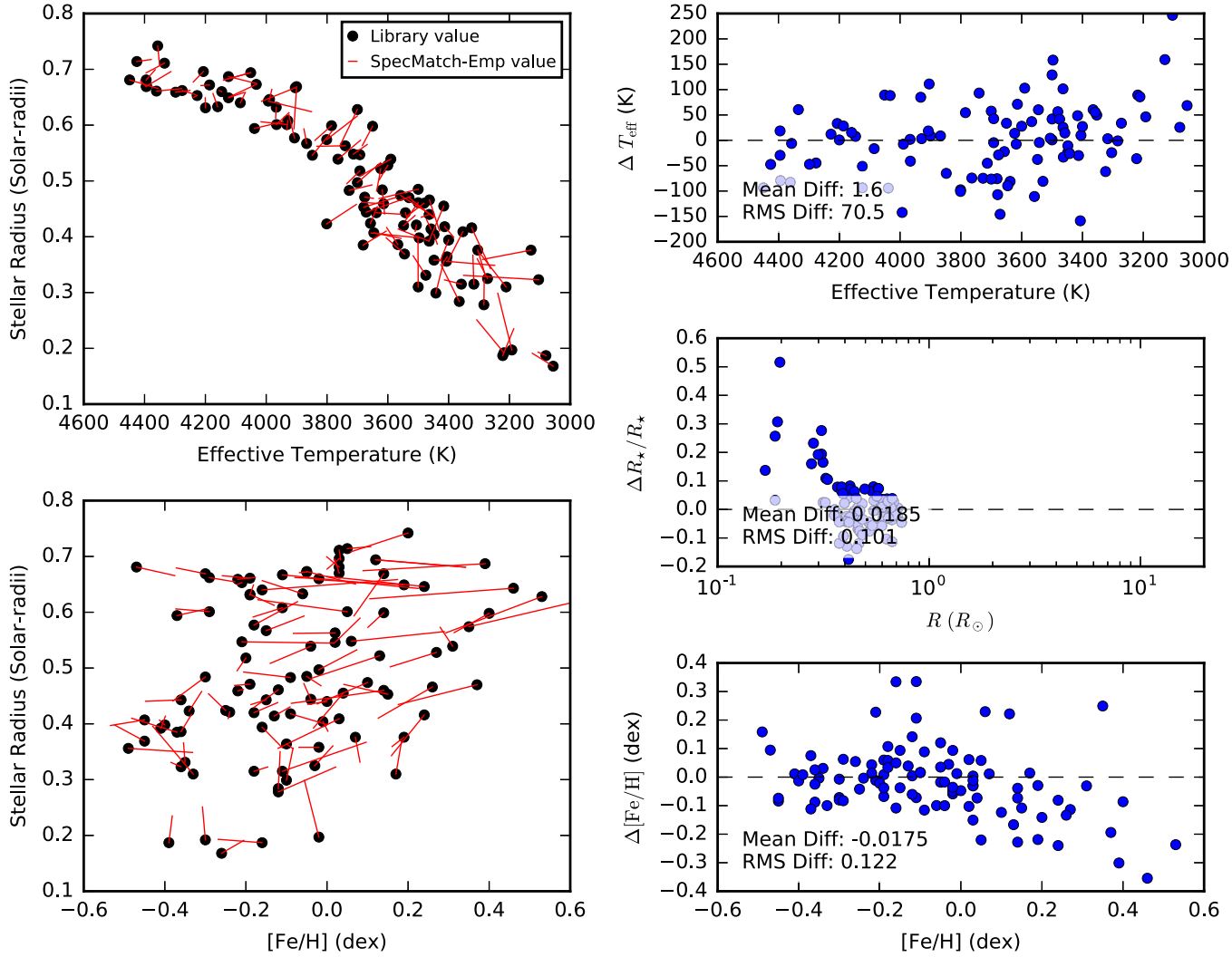

Figure 12. Same as Figure 11, but for the library stars with $T_{\rm eff} < 4500$ K. Performance is improved for this selection of stars due to the more limited spread in main-sequence stellar parameters in the H–R diagram (see Section 4.1).

each star and target S/N. Treating the high-S/N parameter as the ground truth, these results are representative of the random errors of the derived parameters caused by noise in the input spectrum. As expected, the median scatter increases as the S/N decreases. Nonetheless, the median scatter is only 10.4 K in $T_{\rm eff}$, 1.7% in $R_\star$, and 0.008 dex in [Fe/H] even at S/N = 10/pixel. These are significantly smaller than the algorithmic limitations in accuracy from the matching process, demonstrating the robustness of the `SpecMatch-Emp` algorithm even at low S/N. Table 4 lists the scatter in each parameter at different S/Ns.

Furthermore, we note that the increase in scatter with noise is greater for stars with higher $T_{\rm eff}$ and radius. These stars have fewer spectral lines, so random noise has a bigger impact on the derived parameters. The cooler, small stars have much more spectral information in the wavelength region, and so `SpecMatch-Emp` is more robust to noise for these spectra.

4.3. Performance at Low Spectral Resolution

The library spectra were observed with uniform spectral resolution of $R \approx 60{,}000$. Here, we investigate the effect of lower spectral resolutions on the accuracy of the derived parameters. As spectral resolution decreases and narrow lines become washed out, we expect the performance of `SpecMatch-Emp` to worsen since the algorithm relies on matching large numbers of spectral lines against the library spectra.

To perform this study, we use the same subset of 22 stars as in Section 4.2 and simulate lower spectral resolution by convolution with a Gaussian kernel. The degraded spectra were then passed through the `SpecMatch-Emp` routine and a final set of properties was obtained.

Just as in the previous section, we treat the properties obtained using the original high-resolution ($R \approx 60{,}000$) spectra as the ground truth. We plot the absolute difference between these properties and the derived properties from each degraded spectrum in Figure 14. The scatter remains small down to $R = 30{,}000$, with a median of 10 K in $T_{\rm eff}$, 1.3% in $R_\star$, and 0.014 dex in [Fe/H]. At $R = 20{,}000$, the scatter due to the decreased resolution becomes comparable in size to the algorithmic uncertainties determined through our cross-validation study (Section 4.1). At even lower resolutions, `SpecMatch-Emp` is no longer usable, producing very large errors particularly in $T_{\rm eff}$ and $R_\star$. Table 5 summarizes these results.

A closer analysis of the intermediate results reveals that the spectral registration step is fairly insensitive to lower spectral resolution. The same results for the shift, accurate to

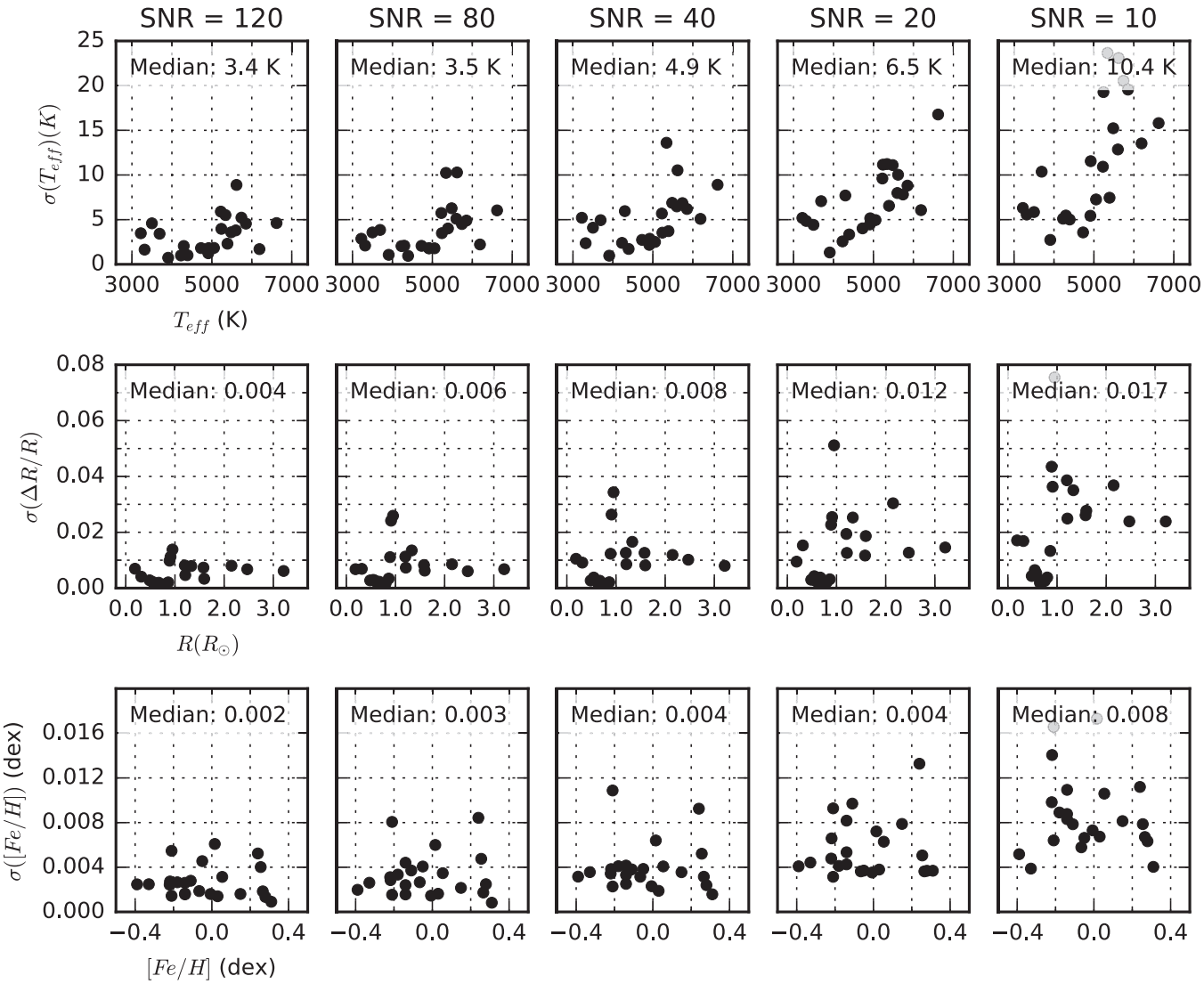

Figure 13. Scatter of parameters derived from SpecMatch-Emp as a function of S/N of the target spectrum, from the study of noise described in Section 4.2. Each point represents the median rms difference between the parameters derived from 22 noisy spectra and the derived parameter of the original, high-S/N spectrum. As S/N decreases, the median scatter increases, and is representative of the effect of photon noise on the precision of `SpecMatch-Emp`. The decrease in precision is most pronounced for stars with greater $T_{\rm eff}$ and radius, because these stars have fewer spectral lines and are thus most susceptible to features being washed out by noise.

Table 4
rms Scatter in Derived Parameters at Different Signal-to-noise Ratios

S/N	$\sigma(T_{\rm eff})$ (K)	$\sigma(\Delta R_\star/R_\star)$	σ([Fe/H]) (dex)
120	3.4	0.004	0.002
80	3.5	0.006	0.003
40	4.9	0.008	0.004
20	6.5	0.012	0.004
10	10.4	0.017	0.008

approximately one pixel, are obtained for most orders even at $R = 10{,}000$.

The performance of `SpecMatch-Emp` suffers during the matching step. In the current implementation of `SpecMatch-Emp`, we do not account for the spectrometer's instrumental profile. As a result, at lower resolution, the algorithm favors increased rotational broadening to account for the broader lines. This compensation by higher rotational broadening works well down to $R \approx 20{,}000$, beyond which it fails for two reasons. First, the kernels associated with rotational broadening and the instrumental profile are different. Second, during the matching step, we do not allow the broadening kernel to exceed $v \sin i = 10$ km s^{-1}. At a resolution of $\sim$10,000 the instrumental profile has a width of $\sim$13 km s^{-1}, which is above the maximum $v \sin i$ allowed during our fitting.

As a result, at spectral resolutions below 20,000, no reference spectrum can be broadened sufficiently to simulate the wider point-spread function of the spectrometer, and the matching algorithm produces a large number of similarly poor matches. The χ^2 surfaces no longer have sharp minima and the final parameters obtained are less accurate. This decrease in performance particularly affects stars with low $T_{\rm eff}$ and $R_\star$. These M and K dwarfs have many narrow but overlapping lines in their spectra (e.g., Figure 3), which get smeared out into a continuum as the resolution decreases, preventing accurate matching with the library spectra. The spectra from hotter stars have fewer but broader lines, which remain visible even in lower resolution spectra.

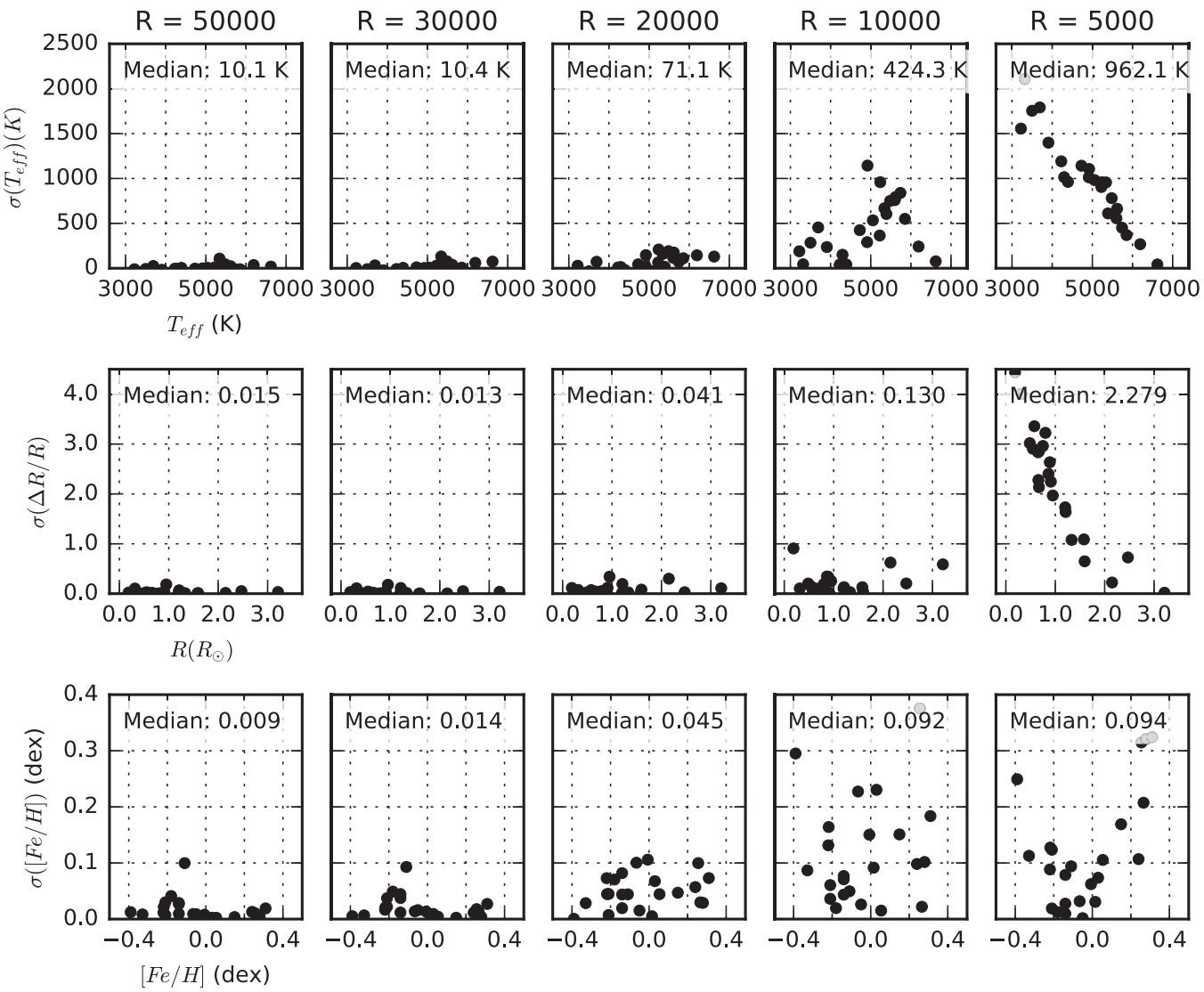

Figure 14. Absolute difference between the parameters derived from the spectra with degraded spectral resolution and those derived from the original high-resolution spectra, analogous to Figure 13. `SpecMatch-Emp` remains accurate down to $R \approx 30{,}000$, beyond which the performance degrades rapidly (see Section 4.3).

While we have made no explicit treatment of spectrometer instrumental broadening, the current implementation of `SpecMatch-Emp` is relatively insensitive to spectral resolutions down to $R \approx 30{,}000$. Difficulties in modeling spectra with $R \lesssim 20{,}000$ could be addressed by proper treatment of the instrumental broadening profile. We welcome community contributions in this respect.

5. Conclusions

We have compiled a library of high-resolution, high-S/N optical spectra of 404 touchstone stars with well-measured properties. The `SpecMatch-Emp` routine is able to rapidly extract fundamental properties of a star from its optical spectrum by comparison against this library. The density of the library and the quality of the associated stellar parameters enable `SpecMatch-Emp` to achieve accuracies of 100 K in $T_{\rm eff}$, 15% in $R_\star$, and 0.09 dex in [Fe/H]. By incorporating information from across a large wavelength range, the algorithm is relatively robust to photon noise and can be readily applied to stellar spectra with S/N as low as 10/pixel.

Table 5
Median Scatter in Derived Parameters at Different Spectral Resolutions

R	$\sigma(T_{\rm eff})$ (K)	$\sigma(\Delta R_\star/R_\star)$	σ([Fe/H]) (dex)
50,000	10.1	0.015	0.009
30,000	10.4	0.013	0.014
20,000	71.1	0.041	0.045
10,000	424	0.13	0.092
5000	962	2.28	0.094

The algorithm also remains robust at lower spectral resolutions until about $R \sim 20{,}000$.

A key advantage of `SpecMatch-Emp` is its accuracy for cool stars with $T_{\rm eff} < 4500$ K. By using empirical, rather than synthetic, spectra to create the library, we have bypassed the difficulties that existing spectral synthesis codes have in modeling the complex spectra of cool stars. Instead, the rich spectral information contained in these stars' spectra is an advantage during the matching process, because the greater number of features improves both the accuracy and precision of

Table 6
SpecMatch-Emp Library

Name	$T_{\rm eff}$ (K)	$R_\star$ ($R_\odot$)	$\log g$ (dex)	[Fe/H] (dex)	$M_\star$ ($M_\odot$)	$\log_{10}$(age/yr)	$\pi_\star$ (mas)	V (mag)	Notes
HD 100623	5140 ± 60	0.720 ± 0.040	4.56 ± 0.05	−0.36 ± 0.05	0.75 ± 0.04	9.81 ± 0.50	104.6	6.0	A1
HD 101904	5883 ± 60	1.540 ± 0.190	4.10 ± 0.05	0.12 ± 0.05	1.12 ± 0.09	9.80 ± 0.11	12.5	8.2	A1
HD 102195	5277 ± 60	0.850 ± 0.050	4.50 ± 0.05	0.10 ± 0.05	0.89 ± 0.04	9.74 ± 0.49	34.0	8.1	A1
HD 102444	5227 ± 60	2.670 ± 0.390	3.60 ± 0.05	−0.00 ± 0.05	1.02 ± 0.21	9.98 ± 0.27	8.5	8.0	A1
HD 102956	4985 ± 60	3.790 ± 0.470	3.38 ± 0.05	0.26 ± 0.05	1.30 ± 0.15	9.70 ± 0.17	8.1	7.9	A1
HD 103459	5722 ± 60	1.710 ± 0.210	4.03 ± 0.05	0.24 ± 0.05	1.15 ± 0.12	9.81 ± 0.15	16.0	7.6	A2
HD 103890	6120 ± 60	1.430 ± 0.160	4.19 ± 0.05	0.03 ± 0.05	1.17 ± 0.07	9.63 ± 0.09	13.7	8.0	A1
HD 104437	5761 ± 60	1.030 ± 0.090	4.40 ± 0.05	0.17 ± 0.05	1.03 ± 0.04	9.64 ± 0.35	16.6	8.6	A1
HD 106088	5470 ± 60	2.070 ± 0.260	3.87 ± 0.05	0.34 ± 0.05	1.23 ± 0.12	9.75 ± 0.13	10.3	8.4	A1
HD 107181	5628 ± 60	1.640 ± 0.210	4.05 ± 0.05	0.31 ± 0.05	1.13 ± 0.12	9.86 ± 0.15	12.5	8.4	A1

Notes. Properties of stars in the `SpecMatch-Emp` library assembled from literature sources and this work.
[A] Sample of Brewer et al. (2016) (Section 2.1.3). $T_{\rm eff}$, $\log g$, [Fe/H] from single line fits to stellar models; $M_\star$, $R_\star$, age from `isochrones`.
[B] Asteroseismic sample from Bruntt et al. (2012) (Section 2.1.4). $\log g$ from asteroseismic analysis; $T_{\rm eff}$ and [Fe/H] from individual spectral line fits; $M_\star$, $R_\star$ and age from `isochrones`.
[C] New K-dwarf sample (Section 2.2). $T_{\rm eff}$ from empirical $V-K$ color–temperature relationship; $R_\star$ from combining $T_{\rm eff}$ with parallax, and $F_{\rm bol}$ calculated from SED fitting; [Fe/H] from SME fitting in Gaidos et al. (2013); $M_\star$, $\log g$, age from `isochrones`.
[D] Sample of Mann et al. (2015) (Section 2.1.2). $T_{\rm eff}$ from stellar atmosphere models; $R_\star$ from combining $T_{\rm eff}$ with $F_{\rm bol}$ obtained from flux-calibrated spectra; [Fe/H] and $M_\star$ from empirical relationships; $\log g$ calculated directly from $R_\star$ and $M_\star$; age from `isochrones`.
[E] Interferometric sample, as compiled in von Braun et al. (2014) (Section 2.1.1). $R_\star$ from optical and infrared interferometry; $T_{\rm eff}$ and [Fe/H] by a variety of methods; $M_\star$, $\log g$ and age from `isochrones`.
[1] Parallaxes from *Gaia* DR1 (Gaia Collaboration et al. 2016).
[2] Parallaxes from *Hipparcos* (van Leeuwen 2007).
[3] No parallaxes found.

(This table is available in its entirety in machine-readable form.)

the derived parameters. We expect that `SpecMatch-Emp` will be a valuable tool for efficiently characterizing large numbers of late-type stars. Such characterization work will be a key observational follow-up effort for future transit surveys such as *TESS* (Ricker et al. 2014) that have an emphasis on M stars.

The applicability of `SpecMatch-Emp` is limited to the region of stellar parameter space spanned by our library stars, i.e., `SpecMatch-Emp` is not applicable to rapidly rotating stars, young stars, chemically peculiar stars, extremely metal-poor stars, etc. Furthermore, the routine's accuracy is limited by the quality of the input parameters. Because the library stars are drawn from the sample of nearby stars, we anticipate that their parameters will be refined with future observations. The `SpecMatch-Emp` library may be easily updated to include these updated parameters, with no modifications to the algorithm.

We thank Tabetha Boyajian, John Brewer, Debra Fischer, Eric Gaidos, Andrew Howard, Howard Isaacson, Heather Knutson, Andrew Mann, and Geoffrey Marcy for enlightening conversations that improved this manuscript. We thank the many observers who collected the Keck/HIRES data used here including R. Paul Butler, Debra A. Fischer, Benjamin J. Fulton, Andrew W. Howard, Howard Isaacson, John A. Johnson, Geoffrey W. Marcy, Kathryn M. G. Peek, Steven S. Vogt, Lauren M. Weiss, and Jason T. Wright. S.W.Y. acknowledges support through the Caltech Summer Undergraduate Research Fellowship program. E.A.P. acknowledges support from a Hubble Fellowship grant HST-HF2-51365.001-A awarded by the Space Telescope Science Institute, which is operated by the Association of Universities for Research in Astronomy, Inc. for NASA under contract NAS 5-26555. This work has made use of data from the European Space Agency (ESA) mission *Gaia* (http://www.cosmos.esa.int/gaia), processed by the *Gaia* Data Processing and Analysis Consortium (DPAC, http://www.cosmos.esa.int/web/gaia/dpac/consortium). Funding for the DPAC has been provided by national institutions, in particular the institutions participating in the *Gaia* Multilateral Agreement. Some of the data presented herein were obtained at the W. M. Keck Observatory, which is operated as a scientific partnership among the California Institute of Technology, the University of California, and the National Aeronautics and Space Administration. The Observatory was made possible by the generous financial support of the W. M. Keck Foundation. Finally, the authors wish to recognize and acknowledge the very significant cultural role and reverence that the summit of Maunakea has always had within the indigenous Hawaiian community. We are most fortunate to have the opportunity to conduct observations from this mountain.

Appendix
Library Stars

The library stars are listed in Table 6.

References

Auvergne, M., Bodin, P., Boisnard, L., et al. 2009, A&A, 506, 411
Baines, E. K., McAlister, H. A., ten Brummelaar, T. A., et al. 2008, ApJ, 680, 728
Baines, E. K., McAlister, H. A., ten Brummelaar, T. A., et al. 2009, ApJ, 701, 154
Borucki, W. J., Koch, D., Basri, G., et al. 2010, Sci, 327, 977
Boyajian, T. S., von Braun, K., van Belle, G., et al. 2013, ApJ, 771, 40
Brewer, J. M., Fischer, D. A., Basu, S., Valenti, J. A., & Piskunov, N. 2015, ApJ, 805, 126
Brewer, J. M., Fischer, D. A., Valenti, J. A., & Piskunov, N. 2016, ApJS, 225, 32
Gaia Collaboration, Brown, A., Vallenari, B., et al. 2016, A&A, 595, A2
Bruntt, H., Basu, S., Smalley, B., et al. 2012, MNRAS, 423, 122
Delfosse, X., Forveille, T., Ségransan, D., et al. 2000, A&A, 364, 217
Dotter, A., Chaboyer, B., Jevremović, D., et al. 2008, ApJS, 178, 89

Gaidos, E., Fischer, D. A., Mann, A. W., & Howard, A. W. 2013, ApJ, 771, 18
Gray, D. F. 1992, The Observation and Analysis of Stellar Photospheres (New York: Cambridge Univ. Press)
Gray, R. O., & Corbally, J. C. 2009, Stellar Spectral Classification (Princeton, NJ: Princeton Univ. Press)
Henry, G. W., Kane, S. R., Wang, S. X., et al. 2013, ApJ, 768, 155
Howard, A. W., Johnson, J. A., Marcy, G. W., et al. 2010, ApJ, 721, 1467
Huber, D., Chaplin, W. J., Christensen-Dalsgaard, J., et al. 2013, ApJ, 767, 127
Kervella, P., Thévenin, F., Morel, P., Bordé, P., & Di Folco, E. 2003, A&A, 408, 681
Kurucz, R. L., Furenlid, I., Brault, J., & Testerman, L. 1984, Solar Flux Atlas from 296 to 1300 nm (Sunspot, NM: National Solar Observatory)
Lindegren, L., Lammers, U., Bastian, U., et al. 2016, A&A, 595, A4
Mann, A. W., Brewer, J. M., Gaidos, E., Lépine, S., & Hilton, E. J. 2013, AJ, 145, 52
Mann, A. W., Deacon, N. R., Gaidos, E., et al. 2014, AJ, 147, 160
Mann, A. W., Feiden, G. A., Gaidos, E., Boyajian, T., & von Braun, K. 2015, ApJ, 804, 64
Mann, A. W., & von Braun, K. 2015, PASP, 127, 102
Michalik, D., Lindegren, L., & Hobbs, D. 2015, A&A, 574, A115
Morgan, W. W., Keenan, P. C., & Kellman, E. 1943, An Atlas of Stellar Spectra, with an Outline of Spectral Classification (Chicago, IL: Univ. Chicago Press)
Morton, T. D. 2015, Isochrones: Stellar Model Grid Package, Astrophysics Source Code Library, ascl:1503.010
Newville, M., Stensitzki, T., Allen, D. B., & Ingargiola, A. 2014, LMFIT: Non-Linear Least-Square Minimization and Curve-Fitting for Python https://doi.org/10.5281/zenodo.11813
Perryman, M. A. C., Lindegren, L., Kovalevsky, J., et al. 1997, A&A, 323, L49
Pickles, A. J. 1998, PASP, 110, 863
Ricker, G. R., Winn, J. N., Vanderspek, R., et al. 2014, Proc. SPIE, 9143, 914320
Sneden, C. A. 1973, PhD thesis, Univ. Texas
Torres, G., Andersen, J., & Giménez, A. 2010, A&A Rv, 18, 67
Valenti, J. A., & Fischer, D. A. 2005, ApJS, 159, 141
Valenti, J. A., & Piskunov, N. 1996, A&AS, 118, 595
van Belle, G. T., & von Braun, K. 2009, ApJ, 694, 1085
van Leeuwen, F. 2007, A&A, 474, 653
Vogt, S. S., Allen, S. L., Bigelow, B. C., et al. 1994, Proc. SPIE, 2198, 362
von Braun, K., Boyajian, T. S., Kane, S. R., et al. 2011a, ApJL, 729, L26
von Braun, K., Boyajian, T. S., Kane, S. R., et al. 2012, ApJ, 753, 171
von Braun, K., Boyajian, T. S., ten Brummelaar, T. A., et al. 2011b, ApJ, 740, 49
von Braun, K., Boyajian, T. S., van Belle, G. T., et al. 2014, MNRAS, 438, 2413